3.9.4.2 Global Model. Both forms of the Global model employ a term which can be related to the effective path length. For the path averaging technique (Global Prediction Model)

$$L_e = \frac{H}{\sin \theta} \gamma(D) R_p^{-\delta(D)} \qquad (3.9\text{-}7)$$

where R_p is the point rain rate, H is the height of the 0°C isotherm, D is the basal distance and γ and δ are the path averaging factors defined in Section 3.4. For a 45° elevation angle at a sea-level ground station near 40°N latitude

$$L_e = 9.14\ R_p^{-0.14} \text{km} \qquad (3.9\text{-}8)$$

For the variable isotherm height form of the Global model,

$$L_e = \frac{1}{\cos \theta} \left[\frac{e^{UZb} - 1}{Ub} - \frac{X^b e^{YZb}}{Yb} + \frac{X^b e^{YDb}}{Yb} \right] \qquad (3.9\text{-}9)$$

where the terms are defined in Section 3.4.3.2. The value of L_e is a complex function of R_p since U, X, Y and Z (implicitly) are functions of R_p.

3.9.4.3 Two-Component Model. Two effective path lengths could be identified in the T-C Model: one for convective cellular rain and one for debris. Differing 0°C isotherm heights are computed for the two types of rain which form a basis for the differing effective path lengths. The lateral modeling of rain also differs for the two rain modes: cellular rain effective path length must be modified to include nearby debris contributions, whereas debris rain is assumed to be uniform. Thus, no attempt is made to identify a single parameter L_e in the T-C Model.

3.9.4.4 CCIR Model. The CCIR Model directly employs the concept of effective path length. The (corrected) 0°C isotherm height is used to define the vertical extent of rain. A slant path length reduction factor is used to adjust the physical path length through rain to account for the horizontal non-uniformity of rain. The resulting effective path length applies only for 0.01% of the time. The attenuation predictions for other time percentages are determined directly from the 0.01% value, without reverting to the path length. For this reason, the dependence of effective path length on rain rate is obscure.

3.9.4.5 Lin Model. The Lin model utilizes two techniques for obtaining the average path length. The first is to temporally average the instantaneous rain rate to five minute intervals. The effect of this averaging process in terms of the effective path length comparison is unclear. However, as will be shown, the other parameter agrees well with the results of other models. Specifically Lin (1978) finds that

$$L_e = \frac{4}{\sin\theta}\left[1 + \frac{4(R_p-6.2)}{2636\sin\theta}\right]^{-1}$$

$$= \frac{2636}{659\sin\theta + R_p - 6.2} \qquad (3.9\text{-}10)$$

At θ = 45 degrees the result is

$$L_e = 2636(460 + R_p)^{-1} \qquad (3.9\text{-}11)$$

3.9.4.6 Simple Attenuation Model (SAM). The simple attenuation model does not readily allow definition of a single L_e parameter. Therefore this parameter is not derived.

3.9.4.7 Experimental Measurements. Ippolito (1978) has employed over sixty months of long term attenuation and rain rate statistics at 11.7, 15, 20 and 30 GHz to derive an effective path length based on experimental measures. The result is

$$L_e = \frac{9.065}{\sin\theta} R_p^{-0.296} \text{ km} \qquad (3.9\text{-}12)$$

for elevation angles from 20 to 90 degrees. At 45 degrees elevation angle

$$L_e = 12.82\ R_p^{-0.296} \qquad (3.9\text{-}13)$$

3.9.4.8 Comparison of Effective Path Lengths. Assuming a ground station at sea level, 40 degrees North latitude and observing at 45 degrees elevation angle, the L_e factors are plotted in Figure 3.9-3 for the two forms of the Global model, the Lin model and the experimental results of Ippolito (1978) and CTS results (Ippolito-1979). The latter experimental results (labeled L_e, exp(11.7GHz) in Figure 3.9-3) were scaled from the 29 degree elevation angle measurements made at Greenbelt, MD to CTS, to 45 degrees using the ratio of the cosecants of the two angles. The original data is the annual curve for 1977 and 1978 shown in Figure 3.9-2. This data is the longest set of continuous, single-site effective path length data published to date for CTS and therefore more weight should be given this curve.

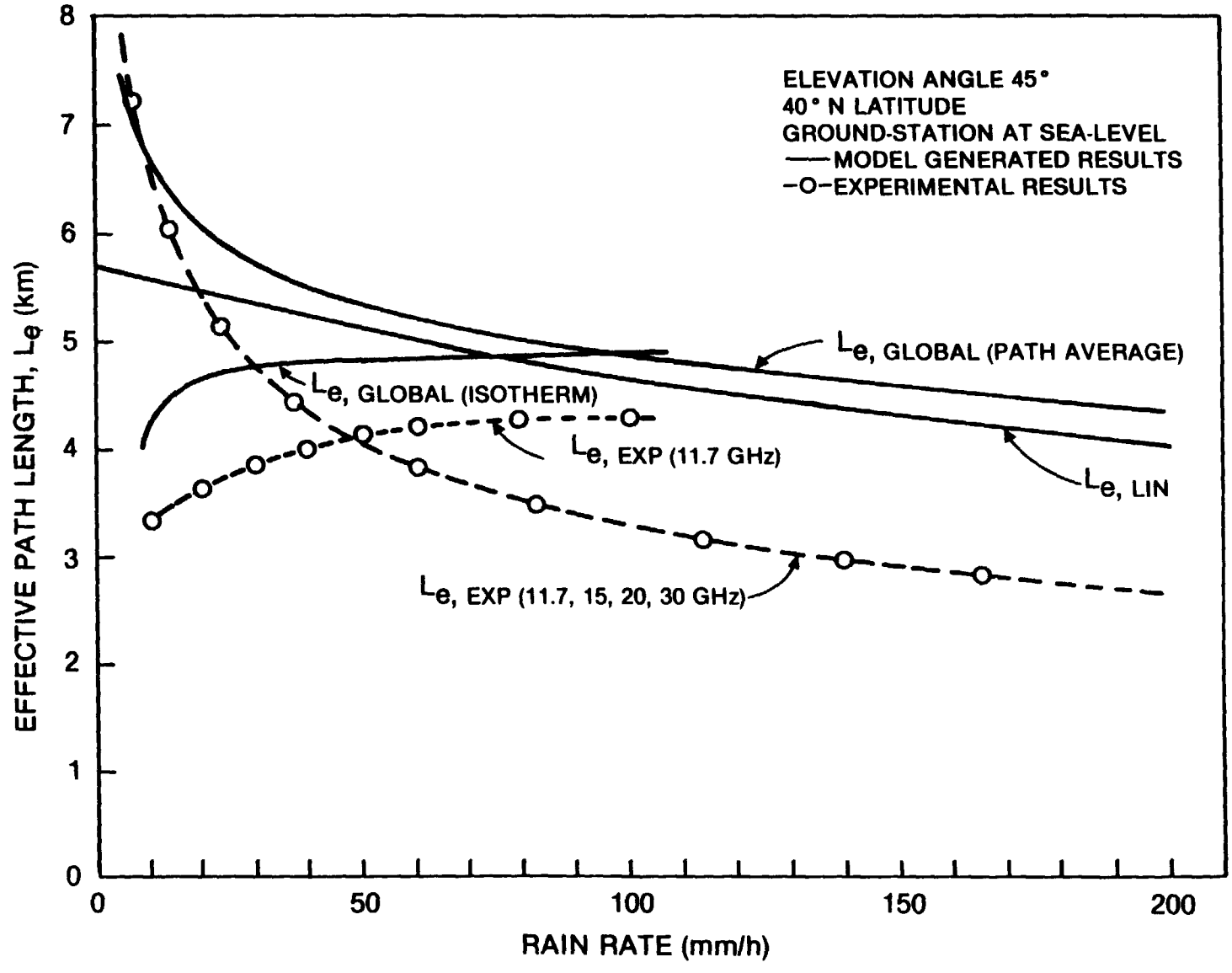

Figure 3.9-3. A Comparison of Effective Path Lengths

The most important result in Figure 3.9-3 is that the use of an effective path length between 4 and 5 kilometers is reasonable. A significant variation occurs below 30 mm/h which may arise due to the presence of winter rains, but this remains unproven. Fortunately for most design problems the most accurate estimates of effective path length are required for annual percentages in the range from 0.01 and 0.001 percent of a year, and in this range both the experimental and model-generated effective path lengths are approximately 4 to 5 km. However, assuming a ± 1 km error bound on L_e the error in estimating L_e is about ± 1dB. If L_e is directly related to the total attenuation, at least a ± 1dB error bound must be placed on the estimate of the path attenuation. This error bound will increase as the elevation angle decreases.

3.10 REFERENCES

Barry, R.C. and R.J. Chorley (1970), Atmosphere, Weather and Climate, Holt, Reinhart and Winston, Inc., New York, p. 205.

Bussey, H.E. (1950), "Microwave Attenuation Statistics Estimated from Rainfall and Water Vapor Statistics," Proc. IRE, Vol. 38, pp. 781-785.

CCIR (1977), "Influence of the Non-Ionized Atmosphere on Wave Propagation," CCIR Study Groups Period 1974-1978, DOC. 5/169-E, May 10 United States of America, Modification to Report 233-3 (REV. 76).

CCIR (1978), "Propagation in Non-Ionized Media", Volume V, XIV Plenary Session, Kyoto, Japan.

CCIR (1978a), Special Preparatory Meeting (WARC-79) Documents.

CCIR (1982a), "Propagation Data Required for Space Telecommunications Systems," Report 564-2, in Volume V, Recommendations and Reports of the CCIR - 1982, International Telecommunications Union, Geneva.

CCIR (1982b), "Prediction of Attenuation Due to Rain on an Earth-Space Path," CCIR Interim Working Party (IWP) 5/2 Meeting, June 1982, Geneva.

CCIR (1982c), "Technical Bases for the Regional Administrative Radio Conference - 1983 for the Planning of the Broadcasting Satellite Service in Region 2," Report of the CCIR Conference Preparatory Meeting, Geneva, 28 June - 9 July 1982.

CCIR (1985a), "Radiometeorological Data," Report 563-2 (MOD F), Study Group 5 Inputs to XVth Plenary Assembly, Document 5/1017, 6 Nov. 1985.

CCIR (1985b), "Propagation Data and Prediction Methods Required for Earth-Space Telecommunication Systems," Report 564-2 (Mod-F), Study Group 5 Inputs to XVth Plenary Assembly, Document 5/1040, 28 Nov. 1985.

CCIR (1986a), "Radiometeorological Data," Report 563-3, in Volume V, Recommendations and Reports of the CCIR - 1986, International Telecommunications Union, Geneva.

CCIR (1986b), "Propagation Data and Prediction Methods Required for Earth-Space Telecommunication Systems," Report 564-3, in Volume V, Recommendations and Reports of the CCIR - 1986, International Telecommunications Union, Geneva.

Chu, T.S. (1974), "Rain Induced Cross-Polarization at Centimeter and Millimeter Wavelengths," B.S.T.J., Vol. 53, pp. 1559-1579.

Crane, R.K. (1966), "Microwave Scattering Parameters for New England Rain," MIT Lincoln Laboratory Report 426, ASTIA Doc. AD-647798.

Crane, R.K. and D.W. Blood (1979), "Handbook for the Estimation of Microwave Propagation Effects - Link Calculations for Earth-Space Paths," Environmental Research and Technology Rpt. No. 1, Doc. No. P-7376-TRL.

Crane, R.K. (1978), "A Global Model for Rain Attenuation Prediction," Eascon Record, pp. 391-395.

Crane, R.K. (1980a), "Prediction of Attenuation by Rain," IEEE Trans. Comm., Vol. COM-28, No. 9, pp. 1717-1733.

Crane, R.K. (1980b), "Earth-Space and Terrestrial Microwave Propagation - Estimation of Rain Attenuation with the Global Model, "ERT Technical Report P-A414-TR, prepared for NASA Headquarters under Contract NASW-3337 (October 1980).

Crane, R.K. (1982), "A Two-Component Rain Model for the Prediction of Attenuation Statistics," Radio Science, Vol. 17, No. 6, pp. 1371-1387

Dougherty, H.T. and E.J. Dutton (1978), "Estimating Year-to-Year Variability of Rainfall for Microwave Applications," IEEE Trans. Comm., Vol. COM-26, No. 8, pp. 1321-1324.

Drufuca, G. and I.I. Zawadzki (1973), "Statistics of Rain Gauge Records," Inter-Union Commission on Radio Meteorology (IUCRM) Colloquium on "The Fine Scale Structure of Precipitation and Electromagnetic Propagation," Nice, France, Conference Record, Vol. 2.

Dutton, E.J. (1971), "A Meteorological Model for Use in the Study of Rainfall Effects on Atmospheric Radio Telecommunications " Off. Telecomm. Rpt. OT/TRER-24, NTIS No. COM-75-10826/AS, Springfield, Va.

Dutton, E.J. (1977), "Earth-Space Attenuation Prediction Procedures at 4 to 16 GHz," Off. Telcom. Rpt. 77-123.

Dutton, E.J. and H.T. Dougherty (1973), "Modeling the Effects of Clouds and Rain Upon Satellite-to-Ground System Performance," Off. Telecom. Report 73-5, NTIS No. COM-75-10950, Springfield, Va.

Dutton, E.J. and H.T. Dougherty (1979), "Year-to-Year Variability of Rainfall for Microwave Aplications in the U.S.A.," IEEE Trans. Comm., Vol. COM-27, pp. 829-832.

Dutton, E.J. and H.T. Dougherty (1984), "A Second Modeling Approach to Year-to-Year Rainfall Variability in the U.S.A. for Microwave/Millimeter Wave Applications," IEEE Trans. Comm., Vol. COM-32, No. 10, pp. 1145-1148.

Dutton, E.J., H.T. Dougherty and R.F. Martin, Jr. (1974), "Prediction of European Rainfall and Link Performance Coefficients at 8 to 30 GHz," Off. Telecom., Dept. of Commerce, NTIS No. AD/A-000804, Springfield, Va.

Dutton, E.J., H.K. Kobayashi, and H.T. Dougherty (1982), "An Improved Model for Earth-Space Microwave Attenuation Distribution Prediction," Radio Science, Vol. 17, No. 6, pp. 1360-1370.

Freeny, A.E. and J.D. Gable (1969), "A Statistical Description of Intense Rainfall," B.S.T.J., Vol. 48, No. 6, pp. 1789-1851.

Goldhirsh, J. and I. Katz (1979), "Useful Experimental Results for Earth-Satellite Rain Attenuation Modeling," IEEE Trans. Ant. Prop., Vol. AP-27, No. 3, pp. 413-415.

Gray, L.F. and M.P. Brown, Jr. (1979), "Transmission Planning for the First U.S. Standard C (14/11-GHz) INTELSAT Earth Station," Comsat Tech. Rev., Vol. 9, No. 1, pp. 61-89.

Hyde, G. (1979), private communication.

Ippolito, L.J. (1978), "Rain Attenuation Prediction at 10 to 100 GHz from Satellite Beacon Measurements," Abstract, Record, EASCON '78, September 25-27, Arlington, Va.

Ippolito, L.J. (1979), "11.7 GHz Attenuation and Rain Rate Measurements with the Communications Technology Satellite (CTS)," NASA TM 80283.

Ippolito L.J. (1986), Radiowave Propagation in Satellite Communications, Van Nostrand Reinhold, New York, p. 88.

Janes, H.B., J.T. Collins and F.K. Steele (1978), "A Preliminary Catalog of Programs and Data for 10-100 GHz Radio System Prediction," Off. Telecomm. Rpt. 78-141.

Jorgenson, D.L., W.H. Klein and C.F. Roberts (1969), "Conditional Probabilities of Precipitation Amounts in the Conterminous United States," U.S. Dept. Comm., Env. Sci. Serv. Ad., Weather Bur., Silver Spring, Md., ESSA Tech Memo WBTM-T DL-18.

Kaul, R., D.V. Rogers and J. Bremer (1977), "A Compendium of Millimeter Wave Propagation Studies Performed by NASA," ORI Final Report, prepared under NASA Contract NAS5-24252.

Kheirallah, H.N., J.P. Knight, R.L. Olsen, K.S. McCormick and B. Segal (1980), "Frequency Dependence of Effective Path Length in Prediction of Rain Attenuation Statistics," Electr. Letters, Vol. 16, No. 12, pp. 448-450.

Laws, J.O. and D.A. Parsons (1943), "The Relation of Raindrop-Size to Intensity," Am. Geophys. Union Trans., Vol. 24, pp. 274-276.

Lin, S.H. (1973), "Statistical Behavior of Rain Attenuation," B.S.T.J., Vol. 52, No. 4, pp. 557-581.

Lin, S.H. (1977), "Nationwide Long Term Rain Rate Statistics and Empirical Calculations of 11 GHz Microwave Rain Attenuation," B.S.T.J., Vol. 56, No. 9, pp. 1581-1604.

Lin, S.H. (1978), "Empirical Calculation of Microwave Rain Attenuation Distributions on Earth-Satellite Paths," Record, EASCON '78, Arlington, Va., pp. 372-378.

Lin, S.H., H.J. Bergmann, and M.V. Pursley (1980), "Rain Attenuation on Earth-Satellite Paths - Summary of 10-Year Experiments and Studies," BSTJ, Vol. 59, No. 2, pp. 183-228.

Marshall, J.S. and W.M. Palmer (1948), "The Distribution of Raindrops With Size," Jrnl. Meteorology, Vol. 51, pp. 165-166.

Olsen, R.L., D.V. Rogers and D.B. Hodge (1978), "The aR^b Relation in the Calculation of Rain Attenuation," IEEE Trans. Ant. Prop., Vol. AP-26, pp. 318-329.

Oort, A.H. and E.M. Rasmusson (1971), "Atmospheric Circulation Statistics," NOAA Professional Paper No. 5, U.S. Dept. Commerce.

Persinger, R.R., W.L. Stutzman, R.E. Castle and C.W. Bostian (1980), "Millimeter Wave Attenuation Prediction Using a Piecewise Uniform Rain Rate Model," IEEE Trans. Ant. Prop., Vol. AP-28, No. 2, pp. 149-153.

Rice, P.L. and N.R. Holmberg (1973), "Cumulative Time Statistics of Surface Point Rainfall Rates," IEEE Trans. Comm., Vol. COM-21, No. 10, pp. 1131-1136.

Rogers, D.V. and G. Hyde (1979), "Diversity Measurements of 11.6-GHz Rain Attenuation at Etam and Lenox, West Virginia," Comsat Tech. Rev., Vol. g, No. 1, pp. 243-254.

Rogers, R.R. (1972), "Radar-Derived Statistics on Slant-Path Attenuation at 10 GHz," Radio Science, Vol. 7, No. 6, pp. 631-643.

Saleh, A.A.M. (1978), private communication.

Setzer, D.E. (1970), "Computed Transmission Through Rain at Microwave and Visible Frequencies," B.S.T.J, Vol. 49, No. 8, pp. 1873-1892.

Skerjanec, R.E. and C.A. Samson (1970), "Rain Attenuation Study for 15 GHz Relay Design," NTIS, AD-709-348, Springfield, Va.

Steele, F.K. (1979), private communication.

Stutzman, W.L., and Dishman (1982), "A simple model for the estimation of rain-induced attenuation along earth-space paths at millimeter wavelengths," Radio Science, Vol. 17, pp. 1465-1476.

Stutzman, W.L., and Dishman (1984), Correction to "A simple model for the estimation of rain-induced attenuation along earth-space paths at millimeter wavelengths," Radio Science, Vol. 19, p. 946.

Stutzman, W.L., and Yon, K.M. (1986), "A Simple Rain Attenuation Model for Earth-Space Radio Links Operating at 10-35 GHz," Radio Science, Vol. 21, NO. 1, pp. 65-72.

U.S. Dept. of Commerce, "Telecommunications Analysis Services - Reference Guide," National Telecommunications and Information Agency, Institute for Telecommunications Sciences, Spectrum Utilization Division, 325 South Broadway, Boulder, CO, 80303, June 2, 1981.

Vogel, W.J. (1982), "Measurement of Satellite Beacon Attenuation at 11.7, 19.04, and 28.56 GHz and Radiometric Site Diversity at 13.6 GHz," Radio Science, Vol. 17, No.6, pp. 1511-1520.

CHAPTER IV

DEPOLARIZATION ON EARTH-SPACE PATHS

4.1 INTRODUCTION

By using orthogonal polarizations, two independent information channels occupying the same RF frequency band can be transmitted over a single link. This technique is used in satellite communications systems to effectively increase the available spectrum. While the orthogonally-polarized-channels are completely isolated in theory, some degree of interference between them is inevitable, owing to less-than-theoretical performance of spacecraft and Earth station antennas, and depolarizing effects on the propagation path. The main sources of this depolarization at millimeter wave frequencies are hydrometeor absorption and scattering in the troposphere.

4.1.1 Definition of Terms

Frequency reuse satellite communications systems utilize either orthogonal linear or circular polarization states. The orthogonal linear polarization (LP) states are normally referred to as vertical and horizontal, but except for Earth stations at the satellite's longitude, the polarization directions are rotated somewhat from the local vertical and horizontal references. The orthogonal circular states are left-hand and right-hand circular polarization (LHCP, RHCP), differing in the sense of rotation of the electric field vector. The "handedness" is defined as follows: a wave is RHCP if the sense of rotation of the field corresponds to the natural curl

of the fingers of the right hand when the right thumb is pointed along the propagation direction. Likewise for LHCP. Thus a RHCP wave coming out of the paper would have an electric field rotating counterclockwise.

A measure of the degree of interference between the two orthogonally-polarized channels is the crosspolarization discrimination (denoted XPD), defined as follows: Let E_{ij} be the magnitude of the electric field at the receiver that is transmitted in polarization state i and received in the orthogonal polarization state j (i,j=1,2). E_{11} and E_{22} denote the copolarized waves E_{12} and E_{21} refer to the crosspolarized waves. This is illustrated in Figure 4.1-1. XPD is the ratio (in dB) of the power in the copolarized wave to the power in the crosspolarized wave that was transmitted in the same polarization state.

$$XPD = 20 \log \frac{E_{11}}{E_{12}} \qquad (4.1\text{-}1)$$

If state "1" is RHCP and "2" is LHCP, for example, then the XPD is the ratio of the RHCP power to the LHCP power, given that only a RHCP wave was transmitted.

A closely related measure is the crosspolarization isolation (XPI), which compares the copolarized received power with the crosspolarized power that is received in the same polarization state:

$$XPI = 20 \log \frac{E_{11}}{E_{21}} \qquad (4.1\text{-}2)$$

Again letting the states "1" and "2" refer to RHCP and LHCP, the XPI compares the power in the RHCP received wave that was transmitted as RHCP to the power that was transmitted as LHCP. XPI is the

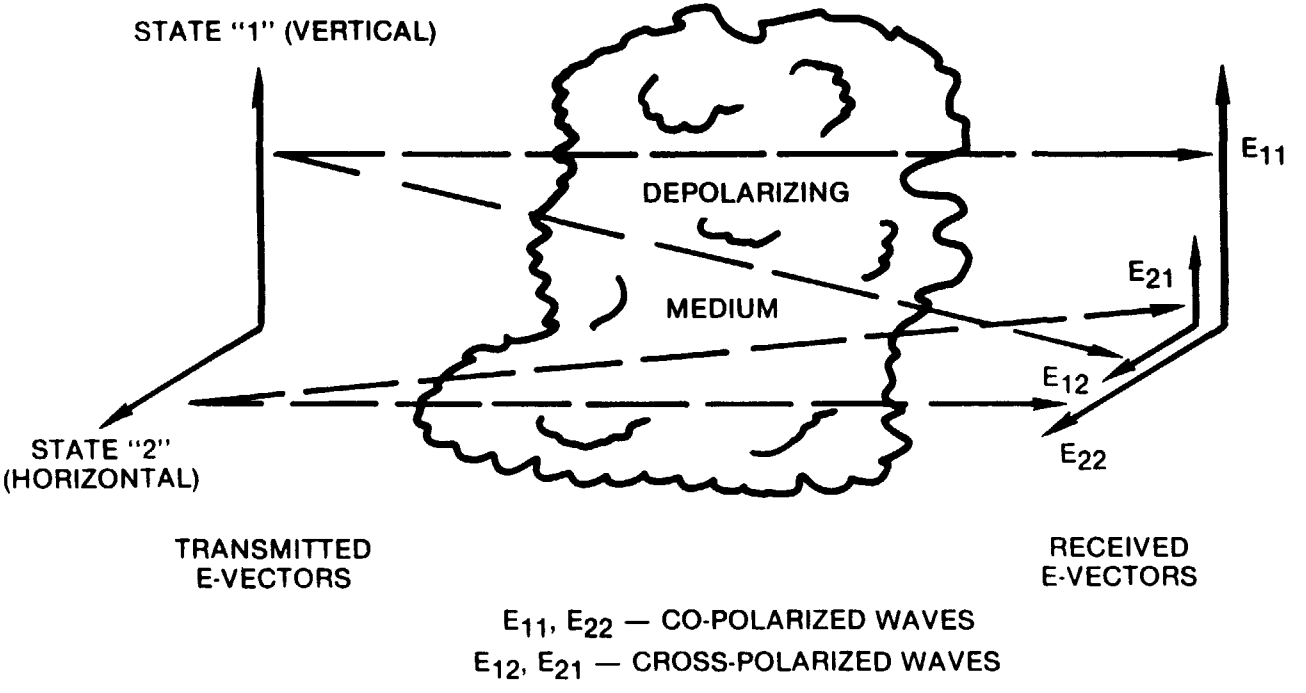

Figure 4.1-1. Definition of Co- and Crosspolarization

parameter that is most meaningful to system engineers, since it directly gives the carrier-to-interference ratio in a received channel. However, XPD is the parameter that is most easily measured. It has been shown (Watson and Arbabi-1973) that XPI and XPD are the same if the hydrometeors responsible for the depolarization have certain symmetry properties. The geometric models that have been used for raindrops and ice crystals have the necessary symmetry, so XPI = XPD in theory. In practice, it has been found that there is not a significant difference between XPI and XPD.

Another term used to describe depolarization, cross polarization ratio (CPR), is the reciprocal of XPD. Other parameters in use, e.g., crosstalk discrimination, crosspolarization distortion, depolarization ratio, crosspolarization level, usually reduce to XPD or XPI.

In the discussion that follows, it is often important to distinguish between polarization properties of a wave in space, and the parameters that we actually measure at the output of the receiver. We shall use XPD to describe the wave properties and a different term, Isolation (I) (after Stutzman-1977) to describe the receiver output. In general,

$$I = \frac{\text{copolarized channel output power}}{\text{crosspolarized channel output power}}$$

Isolation takes into account the performance of the receiver antenna, feed, and other components as well as the propagating medium. When this performance is close to ideal, and/or the XPD of the wave is low (i.e. severe depolarization), then I=XPD. This will be discussed in more detail later.

4.1.2 Hydrometeor Sources of Depolarization

The major sources of depolarization on Earth-space paths are hydrometeors, ionospheric Faraday rotation, and multipath. The

predominant source at millimeter wave frequencies is hydrometeors, and rain is the hydrometeor species that has the greatest effect.

4.1.2.1 Rain. To determine the attenuation due to rain, the raindrops are modelled as spheres of water suspended in space. Real raindrops are falling at their terminal velocity and, due to the complex aerodynamic and hydrostatic forces acting on them, they are in general not spherical. The very small drops (≥0.03 cm in diameter) are very nearly spherical, drops in the range of about 0.03 to 0.10 cm in diameter can be considered oblate spheroids, and drops with diameters larger than about 0.10 cm are asymmetric blobs with flat or concave bottoms (Pruppacher and Pitter-1971). Depolarization occurs because of this lack of spherical symmetry, along with the tendency for the drops to have a preferred orientation (i.e., top and bottom flattened). The effects of the rain-filled medium on a wave propagating through it are dependent on the orientation of the electric field vector with respect to the preferred drop orientation.

It is easy to picture the effect of the "flattened" raindrops on linearly polarized (LP) waves propagatinq horizontally: The fields of horizontal LP waves encounter more water, on the average, than do vertical LP wave fields, and so are subjected to more attenuation and phase shift. An LP wave at some arbitrary orientation, say 45° from the vertical, can be resolved into an equivalent set of component waves having horizontal and vertical polarization. After passing through the rain, the horizontal component has suffered a greater decreased in amplitude, so the polarization direction has been shifted toward the vertical. In addition, the differential phase shift between the components has caused the wave to become slightly elliptically polarized. These depolarizing effects of rain are described more rigorously later.

4.1.2.2 Ice Crystals. Most of the depolarizing effect of rain is produced by differential attenuation. Therefore rain depolarization and attenuation are fairly well correlated. Starting in 1975, when ATS-6 propagation experiments were well underway in Europe,

researchers were surprised to see occasions of severe depolarization that were completely uncorrelated with rain attenuation. The cause of this "anomalous" depolarization has since been identified as oriented ice crystals. Ice can occur at altitudes above the freezing level in cirrus clouds and at the tops of cumulonimbus clouds. When something causes the ice crystal symmetry axes to align themselves, it brings on a polarization-selective phase effect. We are now fairly certain that the electrostatic fields associated with electrically-active storms are at least one aligning force. This is consistent with the observed abrupt changes in XPD coincident with lightning flashes.

Ice depolarization has been theoretically modelled in a manner analogous to rain depolarization. For that purpose, the ice crystals are assumed to be either oblate or prolate ellipsoids, corresponding respectively to "plates" and "needles," which are two distinct types of crystals that are known to exist in clouds. The model is in good agreement with observations and explains the rapid changes in the phase of the crosspolarized waves that accompany lightning flashes.

4.1.2.3 Snow, Graupel and Hail. The anisotropy that is responsible for depolarization by rain and high-altitude ice crystals apparently also exists in snow. From S-band and Ku-band radar measurements, Hendry, et. al. (1976) have observed significant differential phase shifts between the right-and left-hand CP radar returns in moderate to heavy snow. The differential phase shift along the propagation path was found to vary between 0.16° and 1.17° per km at 16.5 GHz, values comparable to that of moderate rainfall. Unlike rain, however, snow produces very little differential attenuation. The differential phase shift in snow should produce measureable depolarization on Earth-space paths, but little or no direct experimental evidence of this has been reported.

Graupel, or snow pellets, may also exhibit some anisotropy, and resulting depolarization. Hail particles, which have a rough

spherical symmetry, probably would not cause depolarization. (McCormick and Hendry-1977).

4.2 MATHEMATICAL FORMULATIONS FOR DEPOLARIZATION

This section presents the mathematical background required to discuss the effects of the propagation medium characteristics and antenna performance on signals in dual polarization Earth-space links. It should enable the system designer to properly interpret experimental data and assess system performance, considering both the medium's depolarizing effects on the wave and the wave's interaction with the antenna system. Most of this development is from Stutzman (1977).

4.2.1 Specifying the Polarization State of a Wave

In the most general case, the tip of the electric field vector of a plane electromagnetic wave traces out an ellipse in the plane perpendicular to the direction of propagation. The polarization state of the wave is given by specifying the shape and orientation of the ellipse, along with the sense of rotation of the field vector. Figure 4.2-1 shows the general polarization ellipse and defines the notation. The electric field vector $\vec{\mathcal{E}}(t)$ is the resultant of sinusoidal components $\mathcal{E}_x(t)$ and $\mathcal{E}_y(t)$ which have different amplitudes E_1 and E_2 and a phase difference δ:

$$\vec{\mathcal{E}}(t) = \hat{x}\,\mathcal{E}_x(t) + \hat{y}\,\mathcal{E}_y(t)$$

$$= \hat{x}\,E_1 \cos\omega t + \hat{y}\,E_2 \cos(\omega t + \delta) \qquad (4.2\text{-}1)$$

where $\hat{x}$ and $\hat{y}$ are unit vectors in the x and y directions, respectively, ω is the radian frequency, and t is time. The polarization ellipse is fully described by the angle, τ, between the ellipse major axis and the x-axis, and the ratio of the major and minor axes of the ellipse. This ratio is the magnitude of an important parameter known as the axial ratio, and is the ratio of

the maximum to the minimum magnitude of the electric field vector. The axial ratio's sign is assigned to be positive if the vector rotation has a left-hand sense and negative for rotation with a right-hand sense: (See Figure 4.2-2.) Linearly polarized waves have an infinite axial ratio; circularly polarized waves have an axial ratio r = ±1, corresponding to LHCP and RHCP respectively.

It is convenient to define another parameter

$$\varepsilon = \cot^{-1} r \quad ; -45^\circ \leq \varepsilon \leq 45^\circ \tag{4.2-2}$$

The specifying parameters ε and τ are related to the quantities used to describe the fields earlier by

$$\varepsilon = \frac{1}{2} \sin^{-1}(\sin 2\gamma \sin\delta) \tag{4.2-3}$$

$$\tau = \frac{1}{2} \tan^{-1}(\tan 2\gamma \cos\delta) \tag{4.2-4}$$

where
$$\gamma = \tan^{-1} \frac{\text{max y-component of } \vec{\mathcal{E}}}{\text{max x-component of } \vec{\mathcal{E}}} = \tan^{-1}(E_2/E_1) \tag{4.2-5}$$

There are other methods used to specify polarization state (Stutzman-1977). The Stokes parameter representation is a matrix formulation. The Poincare sphere is a mapping of polarization states into points on a unit sphere. The complex polarization factor is a single number specifying polarization state. All these various representations are directly relatable to the angles ε and τ, or δ and γ.

4.2.2 Wave-Antenna Interaction

The power available (P_R) at the output of an antenna illuminated by a uniformly polarized incident plane wave of flux density S is

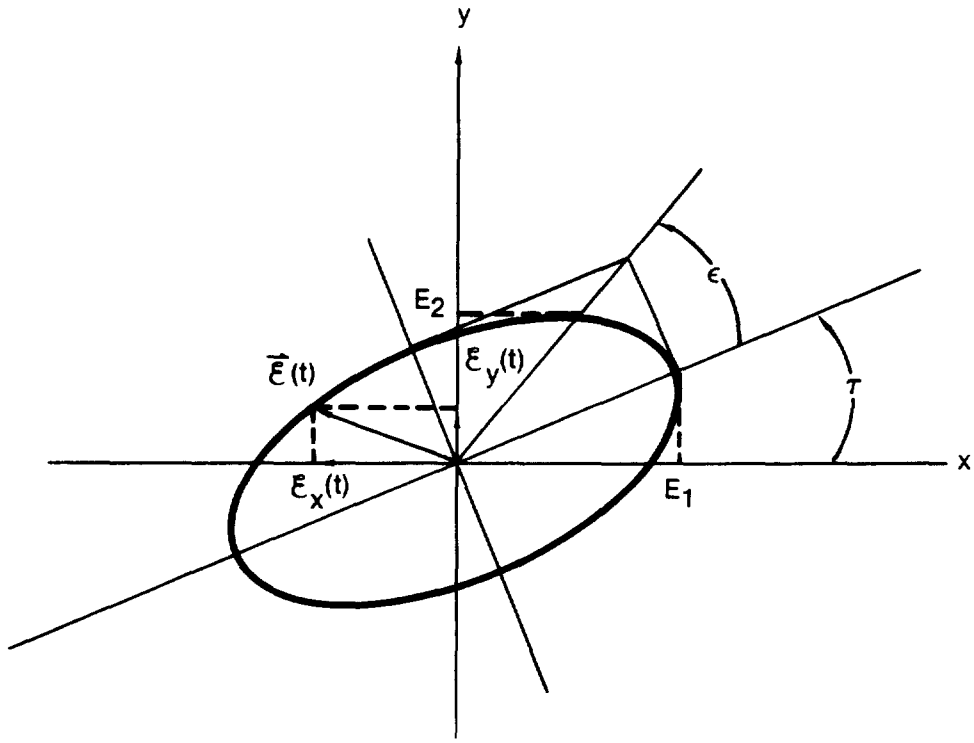

Figure 4.2-1. Polarization Ellipse

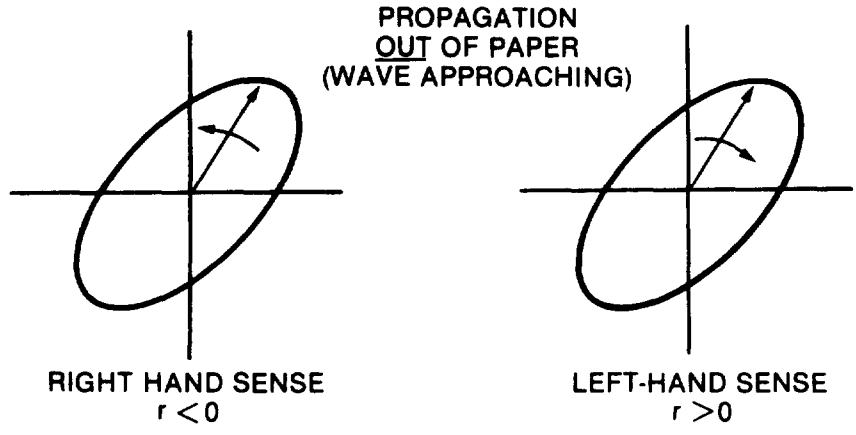

Figure 4.2-2. Definition of Sign of Axial Radio, r

$$P_R = S\ A_e m_p \qquad (4.2\text{-}6)$$

where A_e is the effective aperture of the antenna in the direction of the incident wave, and m_p is the polarization mismatch factor. This factor is a real number between zero and one that depends on the degree of match of the polarization state of the wave and the antenna. The polarization state of a receiving antenna is defined as the state of the wave that the same antenna would transmit, but with time reversed. (A time-reversal changes the direction of propagation of a wave but retains the sense of rotation and axial ratio.) A RHCP incident wave, for example, is perfectly matched to a RHCP antenna. This means the antenna absorbs the maximum amount of power from the wave, and $m_p = 1$. A RHCP antenna absorbs no power from a LHCP wave, and $m_p = 0$. The general expression m_p , assuming arbitrary elliptical polarization states of both the antenna and the wave, is

$$m_p(w,a) = \frac{1}{2} + \frac{4r_w r_a + (r_w^2-1)(r_a^2-1)\cos 2(\tau_a - \tau_w)}{2(r_w^2+1)(r_a^2+1)} \qquad (4.2\text{-}7)$$

where r_a = axial ratio of antenna

r_w = axial ratio of wave

τ_a = major axis angle of antenna

τ_w = major axis angle of wave

We consider some examples to confirm that (4.2-7) is plausible:

Antenna RHCP, Wave LHCP

$r_a = -1,\ r_w = +1$

$$m_p = 1/2 + \frac{4(1)(-1) + (1-1)(1-1)}{2(1+1)(1+1)} = 1/2 - 1/2 = 0$$

Antenna LP, Wave CP

$r_a = \infty$, $r_w = 1$

By dividing the numerator and denominator of the second term of (4.2-7) by r^2_a, then taking the limit as $r \to \infty$, we find that $m_p = 1/2$, which is intuitively agreeable.

Antenna LP, Wave LP

$r_a = r_w = \infty$

Here we divide the numerator and denominator by $r^2_a r^2_w$ and pass to the limit, giving

$$m_p = 1/2 + 1/2 \cos 2(\tau_a - \tau_w) = \cos^2(\tau_a - \tau_w) \qquad (4.2\text{-}8)$$

This equals one when the orientation of the linear polarization axes of the antenna and wave are aligned ($\tau_a - \tau_w$), and equals zero when the axes are orthogonal ($\tau_a - \tau_w = \pm 90^\circ$)

Antenna LP, Wave Elliptically Polarized

$r_a = \infty \qquad r_w = r$

Dividing through by r_a^2 and taking the limit as before, we obtain

$$m_p = 1/2 + \frac{1/2\,(r^2-1)\cos 2(\tau_a - \tau_w)}{2(r^2+1)} \qquad (4\text{-}2.9)$$

Figure 4.2-3 is a polar plot of m_p versus the angle difference $\tau_a - \tau_w$, for r=1.5 and 2.

Letting

$(m_p)_{max} = m_p$ for $\tau_a = \tau_w$ (aligned)

$(m_p)_{min} = m_p$ for $\tau_a = \tau_w + 90^\circ$ (orthogonal)

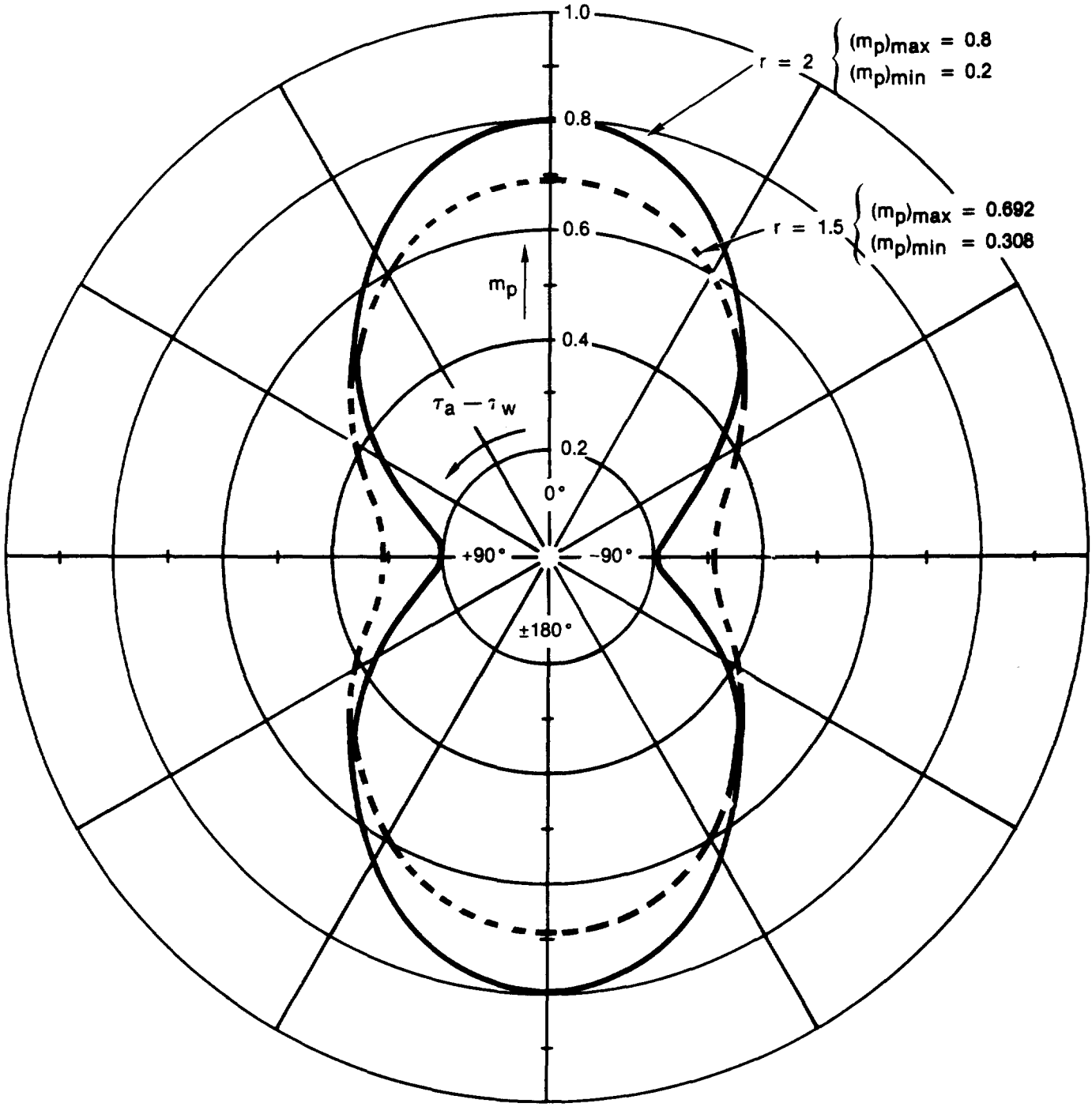

Figure 4.2-3. Polarization Mismatch Factor m_p for LP Antenna and Elliptically Polarized Waves

Some algebra yields

$$r = \left[\frac{(m_p)_{max}}{(m_p)_{min}}\right]^{1/2} \qquad (4.2\text{-}10)$$

This is confirmed in Figure 4.2-3.

This formula suggests a technique for measuring the axial ratio and principal axis orientation of a received wave: The power received by a linearly polarized antenna (e.g., a dipole) is measured as the antenna axis is rotated through 180°. The ratio of **the maximum to the minimum received power, assuming a perfect antenna, is then the square of the axial ratio of the wave, and the orientation of the wave's principal axis is just the antenna's orientation when maximum power is measured.**

4.2.3 Cross Polarization Discrimination (XPD)

Having defined the polarization mismatch factor, we now present a more useful definition of XPD than that given earlier. Orthogonal polarization states are defined, in general, to have axial ratios that are equal in magnitude and opposite in sign (i.e., opposite in rotation sense), and have polarization ellipses with spatially orthogonal axes. Vertical/horizontal LP, and RHCP/LHCP are common examples of orthogonal states. The polarization mismatch factor for a wave with a given polarization state incident on an antenna that is matched to the orthogonal state is zero.

It is always possible to decompose a wave into two components with orthogonal polarization states. An arbitrary wave can be considered as being composed of a component with a polarization state matching the antenna, and a second component with the orthogonal state. The antenna extracts maximum power from the matched component, but completely rejects the orthogonal component. The polarization mismatch factor is then seen to be the proportion

of the total flux density impinging on the antenna that is being carried by the polarization-matched wave component. Denoting the received wave's polarization state by the index w', and the antenna's polarization state by w, the antenna output power is

$$P = SA_e m_p(w', w) \qquad (4.2\text{-}11)$$

A second antenna with equal effective aperture A_e but with a polarization state w_o, that is exactly orthogonal to w, gives an output power

$$P_o = SA_e m_p(w', w_o) \qquad (4.2\text{-}12)$$

The XPD is the ratio of the orthogonal components of the wave,

$$XPD = 10\log [m_p(w', w)/m_p(w', w_o)] \qquad (4.2\text{-}13)$$

assuming that the "w" polarization state is the one the system is designed to maximize, or the copolarized state. The "w_o" state is designated as crosspolarized.

Suppose a LP wave is received, and the copolarized state (w) is designated as horizonally polarized. Let $\tau = \tau_w$, = the angle of the received wave with respect to horizonal. For this case,

$$m_p(w', w) = \cos^2\tau \qquad (4.2\text{-}14)$$

$$m_p(w', w_o) = \sin^2\tau \qquad (4.2\text{-}15)$$

$$XPD = 10 \log (\cot^2\tau) \qquad (4.2\text{-}16)$$

Assume an elliptically polarized wave is received with axial ratio $r_w' = r$, and copolar is designated as LHCP. For this case,

$$r_w = +1, \; r_{w_o} = -1 \qquad (4.2\text{-}17)$$

$$m_p(w', w) = (1/2)\,\frac{(r+1)^2}{r^2+1} \qquad (4.2\text{-}18)$$

$$m_p(w', w_o) = (1/2)\frac{(r-1)^2}{r^2+1} \qquad (4.2\text{-}19)$$

$$XPD = 20 \log [(r + 1)/(r-1)] \qquad (4.2\text{-}20)$$

XPD is plotted versus r for the elliptically polarized case in Figure 4.2-4. An alternate "axial ratio," AR_{dB}, is shown in the figure. This is commonly used and is related to r by

$$ARdB = 20 \log |r| \qquad (4.2\text{-}21)$$

In terms of this parameter, XPD is closely approximated by

$$XPD \approx 24.8 - 20 \log (ARdB) \text{ , for } ARdB < 10 \text{ dB} \qquad (4\ 2\text{-}22)$$

4.2.4 Effect of Non-Ideal Antenna Performance

The XPD describes the polarization characteristics of a received wave with respect to some "copolarized" reference. The true XPD could be measured with an ideal antenna, capable of being matched exactly to the co- and cross polarized state. Actual antennas are not ideal. They can be built with outputs that closely approximate the copolarized and crosspolarized components of the wave, but some degree of degradation is always present in their performance. Here we present a method of quantifyinq the polarization performance of the antenna and taking this performance into account in interpreting polarization measurements.

From this point on, the receive antenna polarization states that are close to the true co- and crosspolarized wave states will be distinguished from the true states by putting their names within quotation marks.